Interplanetary conditions and magnetospheric dynamics during the Cassini orbit insertion fly-through of Saturn's magnetosphere

Caitriona M. Jackman, Nicholas Achilleos, E. Bunce, Baptiste Cecconi, John T. Clarke, S. W. H. Cowley, William S. Kurth, Philippe Zarka

Interplanetary conditions and magnetospheric dynamics during the Cassini orbit insertion fly-through of Saturn's magnetosphere

C. M. Jackman,[1] N. Achilleos,[2] E. J. Bunce,[1] B. Cecconi,[3] J. T. Clarke,[4] S. W. H. Cowley,[1] W. S. Kurth,[3] and P. Zarka[5]

Received 4 February 2005; revised 23 May 2005; accepted 13 July 2005; published 21 October 2005.

[1] The primary purpose of this paper is to discuss the interplanetary conditions that prevailed during the Saturn orbit insertion (SOI) fly-through of Saturn's magnetosphere by the Cassini spacecraft in June–July 2004 and the consequent magnetospheric dynamics. We begin by examining concurrent interplanetary magnetic field (IMF) and Saturn kilometric radiation (SKR) data from Cassini together with images from the Hubble Space Telescope (HST) from an interval in January 2004, which show the effect of the arrival at Saturn of a corotating interaction region (CIR)-related compression region. We then examine the IMF data obtained over five solar rotations bracketing the SOI fly-through and show that a similar CIR compression and embedded crossing of the heliospheric current sheet (HCS) is expected to have impinged on Saturn's magnetosphere at some time during the fly-through. Examination of the IMF direction on either side of the fly-through confirms the HCS crossing. Observations of SKR show relatively weak emissions modulated at the planetary rotation period on the SOI inbound pass. Strong bursts extending to low frequencies, which are not in phase with the previous emissions, were observed on the outbound pass, similar to the CIR-related SKR bursts seen in the January data. We thus suggest that the inbound pass occurred under uncompressed conditions of SKR and auroral quiet, while much of the outbound pass occurred under compressed conditions of SKR and auroral disturbance, probably of the same general character as observed in association with CIR compressions during the HST-Cassini campaign in January 2004. We also examine the in situ magnetic field data observed outbound by Cassini in the predawn sector and find that the largest emission bursts are associated with concurrent variations in the predawn magnetic field, which are indicative of the injection of hot plasma at the spacecraft. Specifically, after an initial field strength increase, the field becomes depressed in strength and highly variable in time. These observations are consistent with an injection of hot plasma into the nightside magnetosphere from the tail, which we suggest is connected with auroral processes of the same nature as observed by the HST during the January 2004 campaign. The injection may be associated with compression-induced reconnection in the tail, as has been proposed to explain the auroral signatures observed in the HST-Cassini campaign data.

Citation: Jackman, C. M., N. Achilleos, E. J. Bunce, B. Cecconi, J. T. Clarke, S. W. H. Cowley, W. S. Kurth, and P. Zarka (2005), Interplanetary conditions and magnetospheric dynamics during the Cassini orbit insertion fly-through of Saturn's magnetosphere, *J. Geophys. Res.*, *110*, A10212, doi:10.1029/2005JA011054.

1. Introduction

[2] Prior to the arrival at Saturn of the Cassini spacecraft on 1 July 2004, the primary source of information concerning the dynamics of Saturn's magnetosphere and its interaction with the solar wind has been from remote sensing studies of the planet's radio emissions, specifically of Saturn kilometric radiation (SKR). SKR is believed to be generated by accelerated auroral electron beams through the cyclotron maser instability [*Lecacheux and Genova*, 1983; *Kaiser et al.*, 1984; *Galopeau et al.*, 1989, 1995; *Zarka*, 1998], and as such provides information on momentum transfer between the magnetosphere and ionosphere via

[1]Department of Physics and Astronomy, University of Leicester, Leicester, UK.
[2]Blackett Laboratory, Imperial College, London, UK.
[3]Department of Physics and Astronomy, University of Iowa, Iowa City, Iowa, USA.
[4]Department of Astronomy, Boston University, Boston, Massachusetts, USA.
[5]Laboratoire d'Etudes Spatiales et d'Instrumentation en Astrophysique, Observatoire de Paris, Meudon, France.

0148-0227/05/2005JA011054

field aligned currents. Variations in these emissions can be used as a remote diagnostic of both rotational and solar wind driven dynamics. Studies have shown that SKR emissions are strongly modulated close to the planetary rotation period [*Kaiser et al.*, 1980]. The exact period has varied by ~1% since first measured by Voyager [*Galopeau and Lecacheux*, 2000], but the current value determined from Cassini SKR observations in 2003–2004 is ~10.75 hours [*Gurnett et al.*, 2005]. Studies with Voyager have also shown that there is a strong positive correlation between SKR and the dynamic pressure of the solar wind [*Desch*, 1982; *Desch and Rucker*, 1983], though the physical mechanism has not been well understood.

[3] In January 2004, a campaign of simultaneous Hubble Space Telescope (HST) UV imaging of Saturn's aurora and Cassini spacecraft measurements of the interplanetary medium upstream of Saturn was undertaken. This included concurrent measurements of the solar wind and interplanetary magnetic field (IMF), together with observations of SKR emissions. This study has shown that Saturn's auroras respond strongly to the magnetospheric perturbations associated with corotating interaction region (CIR) compressions in the interplanetary medium [*Clarke et al.*, 2005; *Crary et al.*, 2005; *Grodent et al.*, 2005; *Bunce et al.*, 2005]. Following a compression, the auroral oval at dawn was observed to expand significantly poleward via the intrusion of bright emissions into the polar region, after which the auroras evolved over ~30 hours into a bright "spiral" form extending from the nightside via dawn into the postnoon sector. Bursts of SKR were also shown to be associated with these compression-induced auroral effects [*Kurth et al.*, 2005], thus corresponding to the solar wind dynamic pressure modulation found previously by *Desch* [1982] and *Desch and Rucker* [1983]. Previous individual images of Saturn's auroras [e.g., *Gérard et al.* 1995, 2004; *Trauger et al.*, 1998; *Cowley et al.*, 2004] have shown similar features, for which the corresponding interplanetary conditions were unknown, while *Prangé et al.* [2004] have recently linked a prenoon auroral disturbance at Saturn to the passage of a coronal mass ejection, tracked from the Sun to Saturn via Earth and Jupiter.

[4] Recently, *Cowley et al.* [2005] have suggested that these auroral and SKR effects are produced by bursts of rapid closure of open flux in Saturn's magnetic tail which are induced by the shock compression of the magnetosphere associated with the CIR. Such bursts are also occasionally observed at Earth [*Petrinec and Russell*, 1996; *Sigwarth et al.*, 2000; *Chua et al.*, 2001; *Boudouridis et al.*, 2003, 2004; *Milan et al.*, 2004; *Meurant et al.*, 2004]. Reconnection in the tail plasma sheet leads to the injection of newly closed flux tubes and hot plasma into the nightside magnetosphere, thus producing an auroral "bulge" in the polar cap, which is then transported by subcorotation with the planet around the outer magnetosphere via dawn, leading to the spiral auroral emission. That compression-induced tail reconnection appears to be a dominant effect at Saturn, as opposed to the primarily substorm-related reconnection at Earth, is taken to be related to the long timescales typically required at Saturn for inflation of the tail with open flux. At Saturn this timescale is typically a week or more [*Jackman et al.*, 2004, 2005], which is thus comparable with the interval between interplanetary compression regions, as opposed to several tens of minutes for a typical substorm "growth phase" at Earth.

[5] The principal purpose of this paper is to discuss observations of magnetic fields and SKR emissions which were obtained during the first "Saturn orbit insertion" (SOI) fly-through of Saturn's magnetosphere by the Cassini spacecraft in June–July 2004. First, however, we examine data from a portion of the January 2004 HST-Cassini campaign interval, specifically that showing the response of the SKR emissions and UV auroras to a CIR-related compression region and embedded heliospheric current sheet (HCS) crossing. We then examine the IMF data that bracket the SOI fly-through and show that a CIR compression region and HCS crossing of similar nature is expected to have impinged on Saturn at some time during the fly-through. The anticipated HCS crossing is indeed confirmed by examination of the IMF data surrounding the fly-through. We then examine the SOI fly-through data itself and show that similar SKR bursts were observed on the outbound pass as were observed during the HST campaign interval, which we thus link to the arrival of the expected CIR compression at Saturn. Finally, we make an initial examination of magnetic field data observed in the predawn nightside magnetosphere concurrently with the first major burst of SKR, and show that the field signature is consistent with the injection of hot plasma at the spacecraft, presumably originating further down the tail. We discuss the implications of these results in relation to the January 2004 HST campaign data, and theoretical ideas on Saturn's solar wind-driven magnetospheric dynamics proposed by *Cowley et al.* [2005].

2. SKR and IMF Measurements During the January 2004 HST-Cassini Campaign

[6] We begin with an overview of a portion of the data from the January 2004 HST-Cassini campaign, which shows the response of the SKR emissions and Saturn's auroras to a CIR compression region and embedded HCS crossing. The discussion given here extends and complements that provided previously by *Clarke et al.* [2005], *Crary et al.* [2005], and *Kurth et al.* [2005].

[7] Figure 1 spans the interval from day 24 to 30 of 2004. Figure 1 (bottom) shows the magnitude of the magnetic field measured by the Vector Helium Magnetometer (VHM) instrument on Cassini [*Dougherty et al.*, 2004]. During the interval shown, the spacecraft was located ~0.2 AU upstream of Saturn in the radial direction, and was also displaced from the planet-Sun line by ~0.5 AU toward dawn. At the beginning of the interval the IMF strength was relatively low at a few tenths of a nT, corresponding to a CIR rarefaction region. At ~1600 UT on day 25 a sudden increase in the field strength was observed, indicative of the arrival at the spacecraft of the forward shock of a CIR compression region, marked in Figure 1 (bottom) by the vertical arrow labeled "S." At ~1500 UT on day 26 a crossing of the HCS took place, indicated by the vertical arrow marked with a "±" symbol. This indicates the time of an enduring reversal of the B_T (azimuthal) component of the IMF in RTN coordinates, from positive to negative. RTN is a right-handed spherical polar system referenced to the Sun's spin axis, in which R is positive radially outward

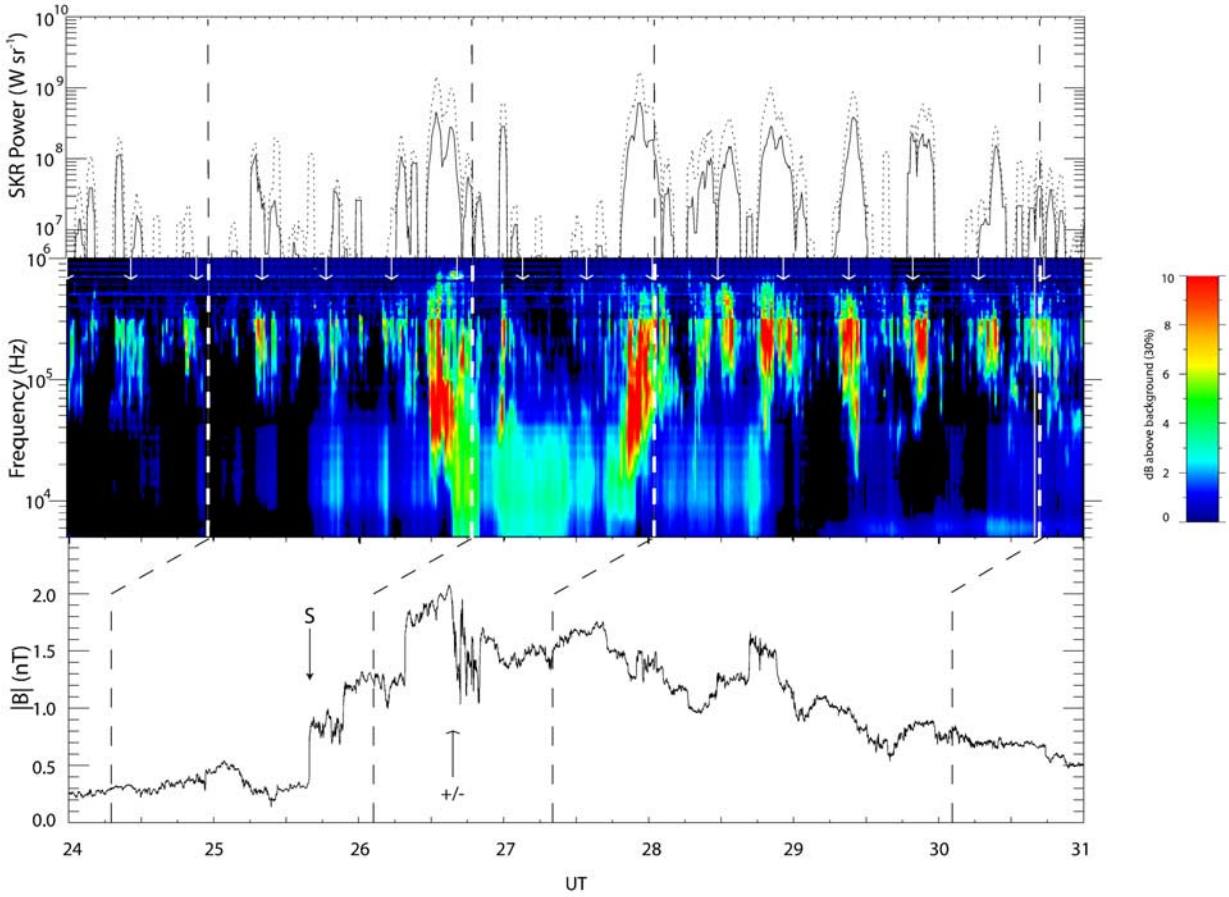

Figure 1. Concurrent Cassini SKR and magnetic field data from a portion of the HST-Cassini campaign in January 2004 for the interval from 24 to 30 January. (top) Inverse-square corrected power of the sum of LH and RH circularly polarized radio waves, where the solid line shows the power in the 100–300 kHz frequency band and the dashed line shows the power in the 4–1000 kHz band. The data are computed every 10 min but are averaged over a 1 hour sliding window. (middle) Corresponding frequency-time spectrogram covering the whole frequency band from 4 to 1000 kHz, color-coded according to the bar on the right-hand side. The vertical arrows are shown at fixed intervals of 10.75 hours and phased with respect to the peaks in periodic emission observed near the beginning of the interval. (bottom) Simultaneous magnitude of the IMF strength observed by Cassini. The vertical dashed lines in Figures 1 (top) and 1 (middle) correspond to the times of the HST images in Figure 1, with a 64 min shift to account for the time of light travel from Saturn to Cassini (SKR) and to the HST (auroral images). The dashed lines in Figure 1 (bottom) have then been shifted by 17 hours to represent the nominal solar wind propagation delay from Cassini to Saturn.

from the Sun, T is the azimuthal direction positive in the direction of planetary rotation, and N is the latitudinal direction positive northward in the solar equatorial plane. Positive B_T thus corresponds to a "toward" sector of the spiral IMF (located north of the HCS during the present solar cycle), and negative B_T to an "away" sector (located south of the HCS). The "±" symbol thus represents a crossing of the HCS from a toward to an away sector, which is, as usual, embedded within an early interval of the compression region. The declining phase of this compression began on day 28, such that by day 30 the field was almost back to rarefaction conditions with IMF strengths of ~0.5–0.7 nT. Overall, the compression region was of ~4 days duration.

[8] Figures 1 (top) and 1 (middle) provide information about the SKR emissions obtained from the Radio and Plasma Wave Science (RPWS) instrument on Cassini [*Gurnett et al.*, 2004]. The SKR data in Figure 1 (top) shows the sum of the powers in left-hand (LH) and right-hand (RH) circularly polarized radio waves in two frequency bands, namely 100–300 kHz (solid line) and 4–1000 kHz (dashed line), though for the present data set the power is strongly dominated by LH emissions. LH polarization corresponds to cyclotron emission from the southern polar region of the planet, which was directed toward the Sun and Cassini during the period of interest. The power detected at the spacecraft has been corrected for distance from Saturn using an inverse square law, assuming for simplicity a source at

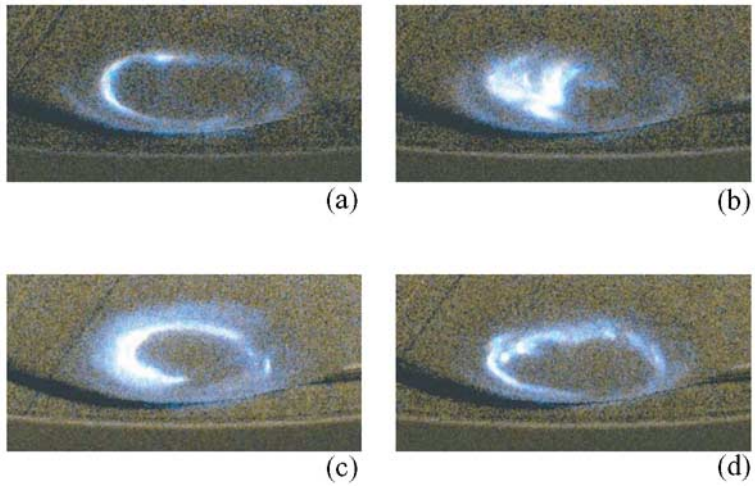

Figure 2. Four UV images of Saturn's southern polar aurora obtained by the STIS instrument on the HST during the interval shown in Figure 1. The noon-midnight meridian is near the center of each frame with noon toward the top, dawn to the left, and dusk to the right. Clear and filtered images from a given HST orbit have been combined in the RGB color system as described in section 3, the total integration time in each frame being ~50 min. The approximate midtimes of the intervals are as follows: (a) 2351 UT on 24 January, (b) 1903 UT on 26 January, (c) 0128 UT on 28 January, and (d) 1902 UT on 30 January.

the center of the planet. The power is then shown in the form of radio power per steradian (W sr^{-1}) in Figure 1 (top), using a log scale. The power has also been averaged (at 10 min resolution) over a sliding 1 hour window. Figure 1 (middle) shows a frequency-time spectrogram over the same interval, covering the frequency band from 4 kHz to 1 MHz, color-coded according to the scale on the right of the plot.

[9] To understand the relationship between the SKR and IMF data, the propagation delays to and from the planet must first be considered. While the SKR propagation time from the planet to Cassini is only a few minutes at the speed of light, and is thus insignificant, appreciable propagation delays occur for the interplanetary medium. Specifically, using an average solar wind speed of 500 km s^{-1}, the radial propagation delay from Cassini to Saturn is ~17 hours. As discussed previously by *Crary et al.* [2005], this timing is unavoidably uncertain to within a few hours, due particularly to nonradial propagation effects and the separation of the spacecraft and planet in heliographic longitude. For disturbances aligned along the nominal Parker spiral direction, for example, the expected propagation delay would be of order ~12 hours. However, 17 hours is used here for simplicity and commonality with previous discussion [*Clarke et al.*, 2005; *Crary et al.*, 2005; *Bunce et al.*, 2005].

[10] At the beginning of the interval, the SKR conditions were quiet, the data showing modulations near the planetary rotation period, as observed previously by Voyager [e.g., *Kaiser et al.*, 1984]. To demonstrate this, we have marked the initial peaks observed in the power plot and spectrogram by vertical arrows in Figure 1 (middle), separated by fixed intervals of 10.75 hours (the current SKR period according to *Gurnett et al.* [2005]), and have continued this across the full width of the plot in order to examine the phasing of the subsequent bursts of emission. On day 26 at ~1200 UT, however, the onset of intense SKR emissions was observed with a spectrum that spreads to lower frequencies, and with peak powers reaching $\sim 1 \times 10^9$ W sr^{-1} [*Kurth et al.*, 2005]. We note from the vertical arrows that this sudden onset occurred at a time when a minimum in power was expected according to the previous phasing of the planetary modulation. This burst occurred ~3 hours after the expected arrival of the forward shock of the CIR compression at Saturn according to the above 17 hours time delay. Following this burst, the usual planetary modulation as observed by Cassini was disrupted for at least two cycles. A brief burst was observed at the end of day 26, some ~40 hours after the arrival of the shock, and again near an anticipated minimum, following which the SKR power remained continuously weak for an interval of ~19 hours, i.e., for almost two planetary rotations. This interval straddles the initial compression region interval containing the HCS crossing. *Kurth et al.* [2005] note, however, that the Unified Radio and Plasma wave experiment onboard the Ulysses spacecraft detected SKR during this interval of apparently weak emissions. They suggest that the beaming was disrupted in some way after the first strong burst, such that the following emissions could not be seen by Cassini. A second burst of high SKR power as observed by Cassini then began at ~1900 UT on day 27, again extending to low frequencies, with peak powers of $\sim 1.5 \times 10^9$ W sr^{-1} (over the full frequency band), and lasting for ~8 hours. This burst again began near the time of an anticipated SKR minimum according to the phasing of the previous modulation, and occurred toward the end of the main high-field compression region interval. Following this second intense burst, the SKR power and frequency range subsequently diminished, while the planetary modulation reemerged with the same phasing (but higher power) as that observed prior to the CIR-related disruption, as indicated by the arrows in Figure 1 (middle). This interval corresponded to the declining phase of the CIR compression.

[11] We now examine four concurrent images of Saturn's UV aurora, Figures 2a–2d, taken by the Space Telescope

Imaging Spectrograph (STIS) on the HST [*Clarke et al.*, 2005], shown in Figure 2. In these images the entire southern auroral oval is visible, due to the 26° tilt of Saturn at this epoch. These frames have been generated by combining individual images obtained on a given HST orbit in the RGB color system. For each date, the frame includes clear images (blue), F25SRF2 filtered images (red), and the mean of all images (green), with a total exposure time of ~50 min (the center times being given in the figure caption). This leads to nearly 30° of rotational blurring for any feature that rigidly corotates with the planet, but distinguishes auroral emissions from reflected sunlight from the disc and rings by their respective blue and red colors. Each frame has a log stretch in intensity, identical for each day, with the upper threshold set to a value of ~20 kR to emphasize the faint emissions.

[12] The vertical dashed lines through Figures 1 (top) and 1 (middle) indicate the timing of the four auroral images relative to the SKR data. The time taken for light to travel between Saturn and Cassini during this interval was ~4 min, and between Saturn and the HST ~68 min, and the lines have been shifted to earlier times accordingly. Similarly, in Figure 1 (bottom) the timing relative to the IMF is indicated by a further shift of 17 hours. It can thus be seen that the HST image in Figure 2a relates to the rarefaction conditions seen at the beginning of the Figure 1 (bottom), during the interval of weak planetary-modulated SKR. It shows a "quiet" auroral oval, with some enhancement in intensity on the dawn (left-hand) side. Figure 2b, taken ~9 hours after the expected arrival of the shock at Saturn, and toward the end of the first intense burst of SKR, shows the effect of the onset of the CIR compression on the aurora. The auroral power had increased by a factor of three from the mean over 8–24 January, with the dawn side oval being completely filled with bright UV emissions, implying active precipitation over the entire dawn side of the polar cap [*Clarke et al.*, 2005]. According to *Cowley et al.* [2005], this is an early effect of the onset of tail reconnection triggered by the sudden CIR compression of the magnetosphere. The HST image in Figure 2c corresponds to a interval ~40 hours after the arrival of the shock, still within the main compression region, but some hours after the peak fields had arrived at Saturn, and toward the end of the second intense SKR burst. The image shows a pronounced spiral form which is brighter in the dawn sector, and with a central roughly circular dark region. According to *Cowley et al.* [2005], such forms result from the rotational transport around the planet of hot plasma injected into the outer nightside magnetosphere from the tail. The final image, Figure 2d, corresponds to an interval toward the end of the compression region where we note that a near-continuous auroral oval had reformed with a central dark polar region, expanded compared with Figure 2c, and with considerable brightness variations in the dawn sector. Overall, we note from this data that in response to a CIR-related compression of Saturn's magnetosphere we observe high-power bursts of SKR that disrupt the pre-existing pattern of planetary-modulated emission, the latter gradually being reestablished over the following 2–3 days. Bright auroral displays are observed simultaneously, which are indicative of hot plasma production in the nightside magnetosphere, followed by rotational transport around the outer magnetosphere via dawn to the dayside and beyond.

3. Cassini IMF Data Surrounding the SOI Fly-Through

[13] We now wish to consider the interplanetary conditions which prevailed during the Cassini SOI fly-through of Saturn's magnetosphere. We begin by considering the structure of the heliosphere during the relevant interval, as revealed by Cassini IMF observations surrounding the fly-through.

3.1. Structure of the Heliosphere During the Approach Phase to Saturn

[14] The structure of the heliosphere during the Cassini approach phase to Saturn has been discussed by *Jackman et al.* [2004], based on observations of the IMF obtained upstream from Saturn during a 6.5 month interval from August 2003 (when magnetic data-taking became almost continuous) to March 2004. SOI then occurred ~4 months later on 1 July 2004 [e.g., *Dougherty el al.*, 2005]. These observations encompassed eight solar rotations at the spacecraft, and showed that the structure of the interplanetary medium generally consisted of two magnetic sectors per solar rotation, with crossings of the HCS usually embedded within few day high-field compression regions (such as that discussed in section 2), separated by several day low-field rarefaction regions. This CIR-related structure is that expected for the declining phase of the solar cycle [e.g., *Gosling*, 1996; *Gosling and Pizzo*, 1999; *Crooker et al.*, 1999]. The main exception occurred during November 2003, when the usual CIR pattern was disrupted by an interval of very strong solar activity. Most recently, *Jackman et al.* [2005] have performed a similar analysis on the Cassini IMF data obtained during the subsequent 5 month interval from March to August 2004, encompassing a further six solar rotations. These data thus span the Cassini SOI fly-through of Saturn's magnetosphere, and show that a similar two-sector structure prevailed during the interval.

3.2. Cassini IMF Data Surrounding the SOI Fly-Through

[15] In this paper, we look specifically at the two solar rotations immediately preceding the SOI fly-through, the fly-through itself, and two solar rotations immediately afterward. In Figure 3 we thus show a stacked plot of Cassini IMF and SKR data for a 4 month interval spanning the SOI fly-through, specifically from day 115 (24 April) to day 242 (29 August) of 2004. The SKR data in Figure 3 will be discussed in section 4 below. Each pair of panels show data from one solar rotation of length 25.5 days, in which the Carrington longitude of the spacecraft decreased from ~360° at the left-hand border of each panel to ~0° at the right-hand border. The data thus encompass five solar rotations at the spacecraft, as indicated by the numbered bars on the right side of the plot. At the beginning of the interval the spacecraft was located at a radial range from Saturn of ~580 R_S (Saturn's radius R_S is taken as 60,330 km), at a local time of ~7.5 hours. Cassini was thus located in the solar wind ~230 R_S upstream from the planet, and displaced ~530 R_S from the planet-Sun line toward

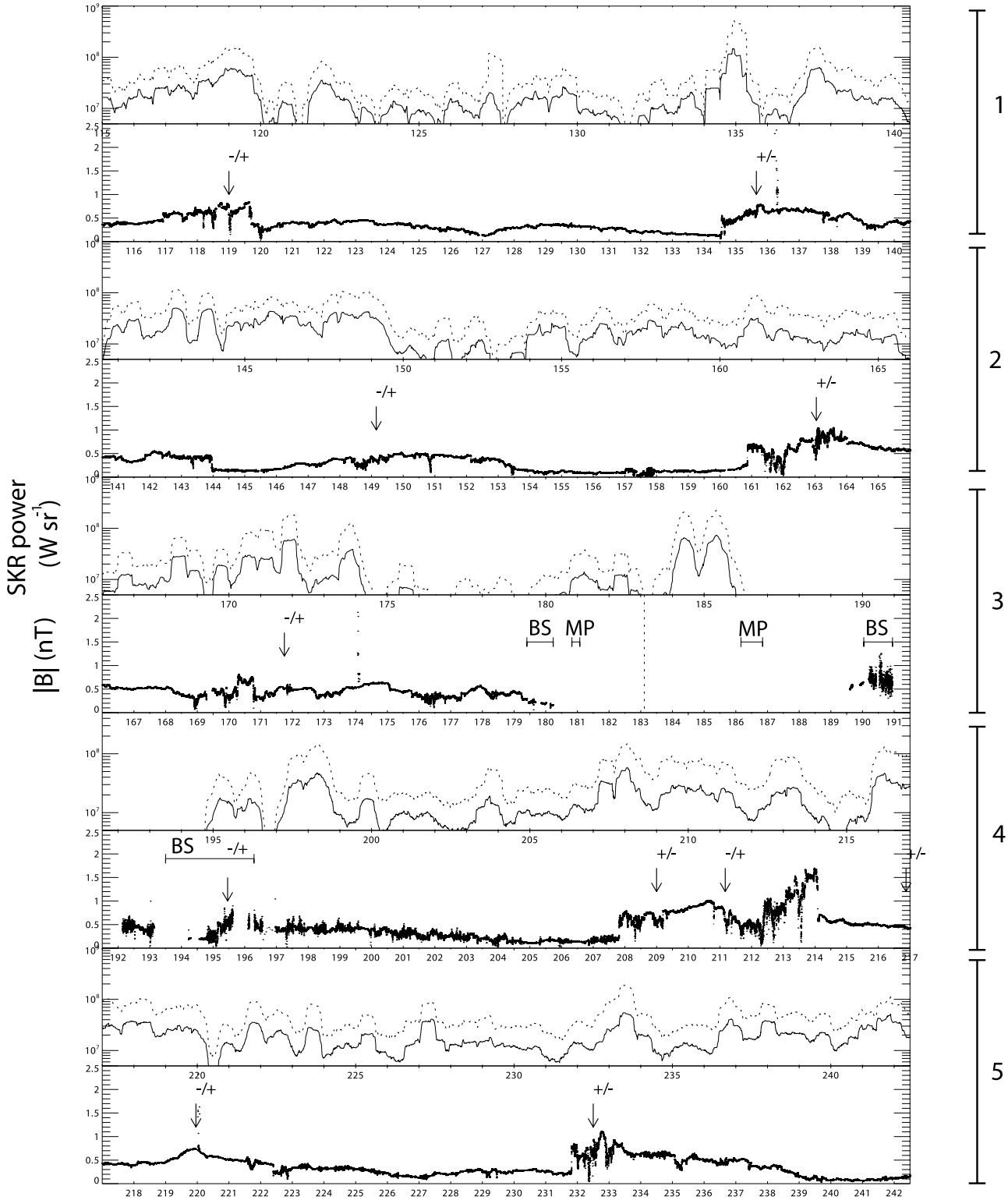

Figure 3

dawn. With a nominal solar wind speed of ~500 km s^{-1}, the propagation delay between spacecraft and planet for purely radial propagation at the solar wind speed was thus ~7.5 hours, reducing to ~5.5 hours for disturbances aligned along the nominal Parker spiral direction. These estimated delays decreased approximately linearly with time as the planet was approached, with closest approach occurring at 0239 UT on day 183 (1 July) at a radial distance of ~1.3 R_S. This time is marked by the vertical dashed line in the central IMF panel. At the end of the interval Cassini had receded to a radial range of ~150 R_S from the planet at a local time of ~6.5 hours, almost on the dawn meridian. The delay for purely radial propagation from the Sun was then less than 0.5 hours, or smaller in magnitude than −0.5 hours for disturbances aligned along the spiral (the minus indicating that such disturbances would arrive at the planet before arriving at the spacecraft). Overall, the interplanetary propagation delay between the spacecraft and the planet during the whole of the interval is thus expected to be no more than a few hours, which is thus small compared with the solar rotation timescale of Figure 3.

[16] The bottom panel of each pair in Figure 3 shows the magnitude of the IMF. Data are omitted during the SOI interval, principally in rotation 3, when the spacecraft was located in either the magnetosheath or magnetosphere of Saturn, though the IMF may be somewhat disturbed by upstream waves in the vicinity of the planetary bow shock [*Dougherty et al.*, 2005]. Intervals during which bow shock crossings were observed are indicated in rotations 3 and 4 by the horizontal bars marked "BS," while intervals containing magnetopause crossings are similarly indicated by the horizontal bars marked "MP." As in Figures 1 and 2, the vertical arrows marked with the "±" and "∓" symbols indicate crossings of the HCS, from toward to away and vice versa. It can thus be seen that the IMF structure generally consisted of two sectors per solar rotation throughout the interval, which, as indicated above, had been the case since (at least) August 2003 [*Jackman et al.*, 2004, 2005]. Comparison with the results of *Jackman et al.* [2004, 2005] also shows that the phasing in heliographic longitude of the crossings had remained roughly constant over the interval. The magnetic field data in Figure 3 show that the HCS crossings are generally embedded in several day regions of higher field strength, peaking typically at ~0.75 to ~1.5 nT, which, as in Figures 1 and 2, we take to correspond to CIR-related regions of solar wind compression (Cassini solar wind plasma data are not routinely available during the interval considered here). The "±" crossings in the right-hand portions of the panels, in particular, all have a well-marked sharp increase in field strength preceding the crossing, which we take to correspond to the "forward" shock of the following CIR compression region, of the same general character as the shock marked "S" in Figure 1, which occurred four solar rotations before the start of the interval shown here. Between the compression regions the field strength then falls typically to values of a few tenths of a nT, corresponding to the intervening solar wind rarefaction regions.

3.3. Implications for Solar Wind Conditions During the Cassini SOI Fly-Through

[17] We now compare the phasing of the CIR-related structures observed during the solar rotations shown in Figure 3 with the timing of the SOI fly-through indicated by the bow shock and magnetopause markers in the IMF panel of rotation 3. The comparison immediately shows that the CIR compression region associated with the "±" crossing of the HCS is expected to have arrived at Saturn's magnetosphere at some time during the SOI fly-through. Judging from the times of the "earliest" and "latest" arrivals of the sharp field increase occurring prior to the HCS crossing in the two preceding and two following solar rotations, it seems probable that the forward shock of the CIR arrived some time between days 181 (29 June) to 185 (3 July) inclusive, a period that brackets essentially the whole of the fly-through interval when Cassini was inside the magnetosphere. The IMF data obtained prior to the final inbound bow shock crossing on day 180 (28 June) show that the compression region had not arrived at that time, such that the initial period of entry to the Saturn system, at the least, occurred during the weak field conditions of a solar wind rarefaction region. This is consistent with the expanded condition of the bow shock and magnetopause observed during the inbound pass [*Dougherty et al.*, 2005]. On exit, however, the IMF strength was elevated to values comparable with those following the compression regions observed during the previous and following solar rotations, indicating that the compression region had indeed arrived while Cassini was inside the magnetosphere. This is also consistent with the relatively compressed condition of the

Figure 3. Stacked plot of Cassini IMF and SKR data obtained from day 115 (24 April) to day 242 (29 August) of 2004, shown as five double panels of 25.5 days duration. Each double panel corresponds to one solar rotation at the spacecraft, as numbered on the right-hand side of the figure. The top panel of each pair shows SKR data, while the bottom panel shows the corresponding IMF data. The SKR data shows the sum of the powers in LH and RH circularly polarized radio waves (corresponding to emissions from Saturn's southern and northern hemispheres, respectively) in two frequency bands, 100–300 kHz (solid line) and 4–1000 kHz (dashed line). The data have been inverse-square corrected for distance from Saturn, assuming for simplicity a source located at the center of the planet, and are presented as power per unit solid angle (W sr^{-1}). The data have also been averaged over intervals of 10.75 hours (computed every 10 min) to smooth the modulation at the planetary rotation period. The magnetic field data show the strength of the IMF, with data being omitted during rotations 3 and 4 when the spacecraft was located either in the magnetosphere or magnetosheath of Saturn during the SOI fly-through. Horizontal bars marked "BS" indicate intervals containing magnetospheric bow shock crossings, while bars marked "MP" indicate intervals containing magnetopause crossings. The vertical dotted line in the IMF panels of rotation 3 shows the time of closest approach to Saturn. Vertical arrows marked with plus and minus symbols indicate the time of enduring changes of the B_T component of the IMF, indicative of crossings of the HCS. The symbol "±" indicates a transition from positive to negative B_T, corresponding to a transition from a "toward" to an "away" sector and vice versa for "∓".

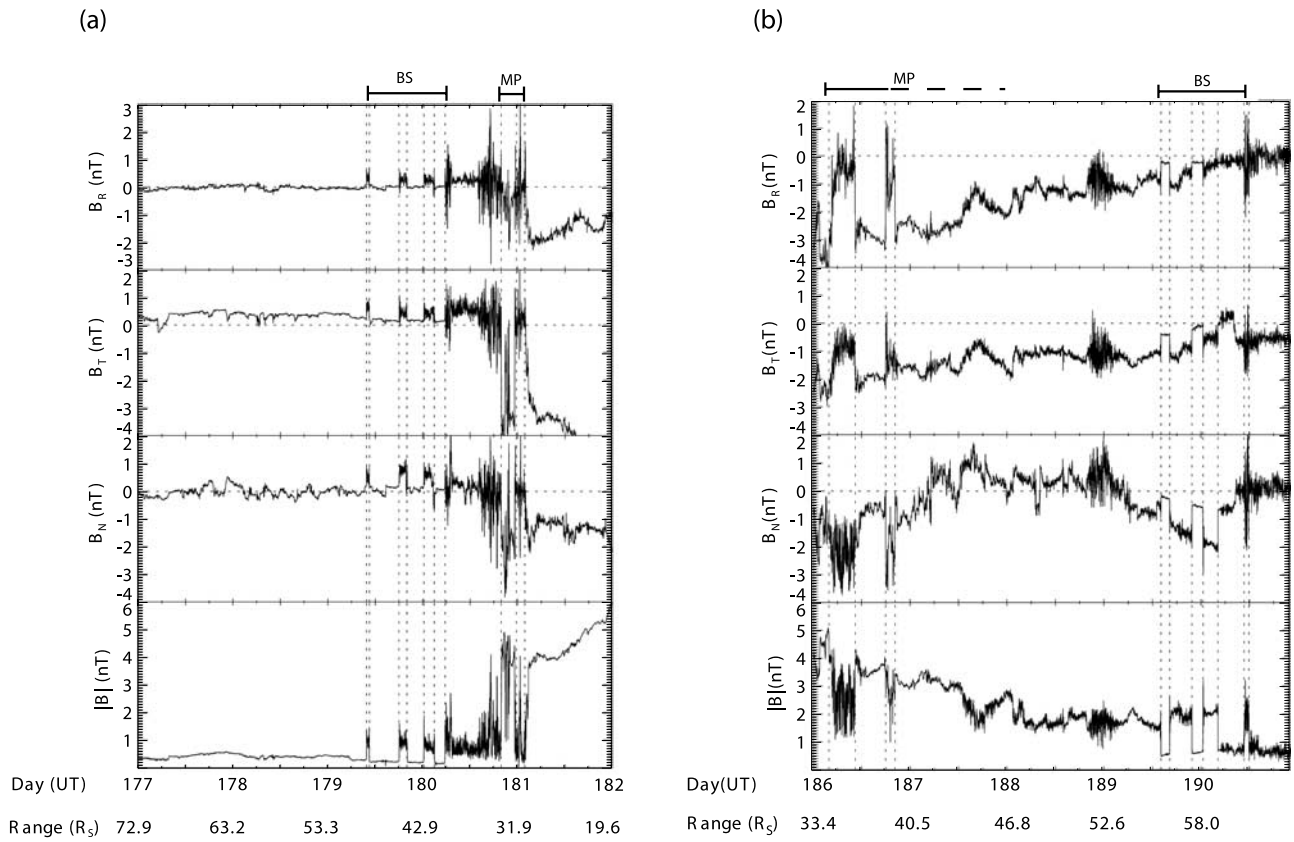

Figure 4. Cassini magnetic field data for two 5-day intervals spanning solar wind, magnetosheath, and magnetosphere regions on the inbound and outbound passes of the SOI fly-through. From top to bottom, the panels show the B_R, B_T, and B_N components of the field in RTN coordinates and the total field strength $|B|$. Vertical dotted lines show the positions of magnetopause and bow shock crossings, as indicated by the horizontal lines marked "MP" and "BS" at the top of the plots. (a) Interval days 177–181 on the inbound pass, spanning the whole interval from the first bow shock crossing on day 179 to the last magnetopause crossing on day 181. The radial distance of the spacecraft decreased from ~73 to ~20 R_S over the interval, at a local time of ~7.5 hours. (b) Interval days 186–190 on the outbound pass, spanning the interval from the first magnetopause crossing on day 186 to the seventh bow shock crossing on day 190. Further shock crossings occurred on days 194–196. The "MP" line at the top of the plot is shown partly dashed because magnetopause encounters occurring on days 187 and 188 remain unclear in the absence of sharp field shears and concurrent plasma data. The radial distance of the spacecraft increased from ~33 to ~63 R_S over the interval, at a local time of ~5 hours.

magnetopause and bow shock observed initially on the outbound pass [*Dougherty et al.*, 2005], as indicated in the third IMF panel of Figure 3. However, further bow shock crossings were observed at rather larger distances on days 194–196 (12–14 July), as marked in the IMF panel during rotation 4, indicative of declining solar wind dynamic pressure and a corresponding expansion of the magnetosphere and bow shock during this interval.

[18] The magnetic field data in Figure 3 thus strongly indicate that a CIR compression region associated with a "±" HCS crossing impinged on Saturn at some point during the interval when Cassini was inside the magnetosphere. If so, we should then find that the sense of the B_T field component in the IMF and magnetosheath should have reversed from positive on the inbound pass to negative on the outbound pass. In Figure 4 we show magnetic field observations in RTN coordinates for two 5 day intervals, the first (Figure 4a) spanning the inbound interval from the first crossing of the bow shock to the last crossing of the magnetopause (days 177 to 181 respectively), while the second (Figure 4b) spans the outbound interval from the first crossing of the magnetopause to the seventh crossing of the bow shock (days 186 to 190 respectively). Crossings of the bow shock and magnetopause are indicated by the dashed vertical lines during intervals marked as "BS" and "MP" at the top of Figure 4. The MP interval on the outbound pass is indicated partially by a dashed line, however, since the absence of a large magnetic shear between the internal and external field during days 187 and 188 renders the timing of the final magnetopause encounter(s) unclear [*Dougherty et al.*, 2005]. In addition, plasma and other science data (excepting magnetometer data) that might contribute to an identification were not obtained on the outbound pass from days 186 to 194, due to a temporary suspension of science commanding for reasons of spacecraft health and safety. Nevertheless, the magnetometer data in Figure 4 show that the B_T field component in the solar wind and magnetosheath was consistently positive

during the inbound pass up to the last magnetopause encounter on day 181, and was consistently negative during the outbound pass from the first magnetopause encounter on day 186. These data thus prove that a "±" crossing of the HCS took place during the intervening interval when Cassini was located continuously inside the magnetosphere, with the further implication that the associated CIR compression also impacted on the system at some time during this interval. These data do not, however, provide an otherwise more detailed indication of the expected timing of the event, and of the associated SKR and auroral effects that should then follow.

4. SKR Data and Its Implications for Magnetospheric Dynamics During the SOI Fly-Through

[19] It has been seen from the discussion of the Cassini-HST campaign data in section 2 that SKR emissions are strongly modulated by the arrival at Saturn of CIR-compressions in the interplanetary medium, as anticipated from the earlier Voyager results of *Desch* [1982] and *Desch and Rucker* [1983]. The primary purpose of this section is thus to examine the SKR data obtained during the SOI interval for related effects, which may thus provide insight into interplanetary-modulated magnetospheric dynamics during the fly-through. We begin, however, by giving an overview of the emissions observed during the interval surrounding the fly-through, which provides a wider context.

4.1. SKR Observations Surrounding the SOI Fly-Through

[20] The top panels in Figure 3 show the inverse-square corrected power in SKR emissions observed over the ~4 month (5 solar rotation) interval surrounding the SOI fly-through, which we compare with the IMF data shown in the same panel, discussed in section 3. We recall from section 3.2 that the solar wind propagation time from the spacecraft to the planet is at most a few hours, while the light propagation time from the planet to the spacecraft is at most a few minutes, such that the two data sets may be considered to be essentially simultaneous on the timescale of this plot. As in Figure 1, the solid line shows the sum of the powers in the LH and RH polarized emissions in the 100–300 kHz frequency band, while the dashed line shows that in the 4–1000 kHz band. The value is again shown in the form of radio power per steradian (W sr^{-1}), using a log scale. The power has also been averaged over a 10.75 hours sliding window in order to smooth the variations associated with the planetary rotation period.

[21] If we first compare the SKR and magnetic field data in Figure 3 when Cassini was in the solar wind, it can be seen that there is a general correspondence between high field strength intervals with embedded HCS crossings and high-power SKR emissions, as anticipated from the results shown previously in section 2 and those of *Desch* [1982] and *Desch and Rucker* [1983]. If we examine the pair of panels corresponding to solar rotation 1, for example, it can be seen that intervals of high SKR power accompany the high field region and HCS crossing on days 118–119, and also the sharp field strength increase associated with the forward shock of the CIR compression occurring on day 134. There is also a further interval of high SKR power during the high-field region following the latter shock, centered on day 137. In rotations 2, 4, and 5 we also note in particular that an interval of stronger SKR emission is again associated with the compression region occurring in the second half of each solar rotation, during which the "±" HCS crossing took place. The emissions start on day 160 in rotation 2, 207 in rotation 4, and 232 in rotation 5. We note that it was this "same" compression region that caused the major SKR and UV auroral effects which were observed during the Cassini-HST campaign discussed in Section 2, such that it seems reasonable to infer from these data that similar magnetospheric and auroral effects were produced during its subsequent appearances in the following solar rotations. This is also the compression that impinged on Saturn during the SOI fly-through, as inferred above, such that related dynamics were also presumably in progress at some point during the fly-through.

[22] We therefore now turn to the SKR data observed during the SOI pass during solar rotation 3 in Figure 3. We note that a major SKR data gap occurred on the outbound pass from days 186 to 194, due to the spacecraft problem noted above, when no science data were obtained other than magnetometer data. This SKR data gap thus spans the interval from near the first outbound magnetopause crossing to near the final outbound bow shock. Fortunately, however, full data coverage extends over nearly all of the magnetosphere traversal up to the first outbound magnetopause crossing on day 186, and thus through all of the interval during which the arrival of the CIR compression appears likely from the contextual magnetic field data discussed in section 3. Examining the SKR data in this panel, it can first be seen that an interval of high-power SKR bursts occurred from days 170 to 173, associated with the disturbed field region surrounding the "∓" HCS crossing that occurred on day 171. Following this, however, an extended interval of very low power SKR emission began on day 174 during the approach to the planet, and continued in the low-field rarefaction region leading up to entry into the Saturn system on day 180. Somewhat higher normalized powers were then observed during the inbound pass through the magnetosphere and during closest approach on days 181–183, though remaining overall of modest normalized amplitude. We note in passing that the SKR power calculations were modified during closest approach because the method of power calculation employed at larger distances, which used a planet-centered source, is inadequate in the region very close to the planet. Specifically, during the interval from day 182.5 to the end of day 183, the powers were derived using the RPWS instrument as a circularly polarized goniometer (assuming no linear polarization), such that the varying source direction, as well as the power, was obtained directly from the data. Bursts of high-power SKR emission were then observed on days 184 and 185, comparable in normalized magnitude to the highest observed at other times during the interval shown in Figure 3, before the beginning of the data gap starting on day 186. In view of the HST-Cassini campaign results discussed in section 2, it seems reasonable to suppose that these bursts are related to auroral events of a similar nature to those shown in Figures 1 and 2, associated with the anticipated CIR-compression of the magnetosphere. Of course we do not know precisely how the onset

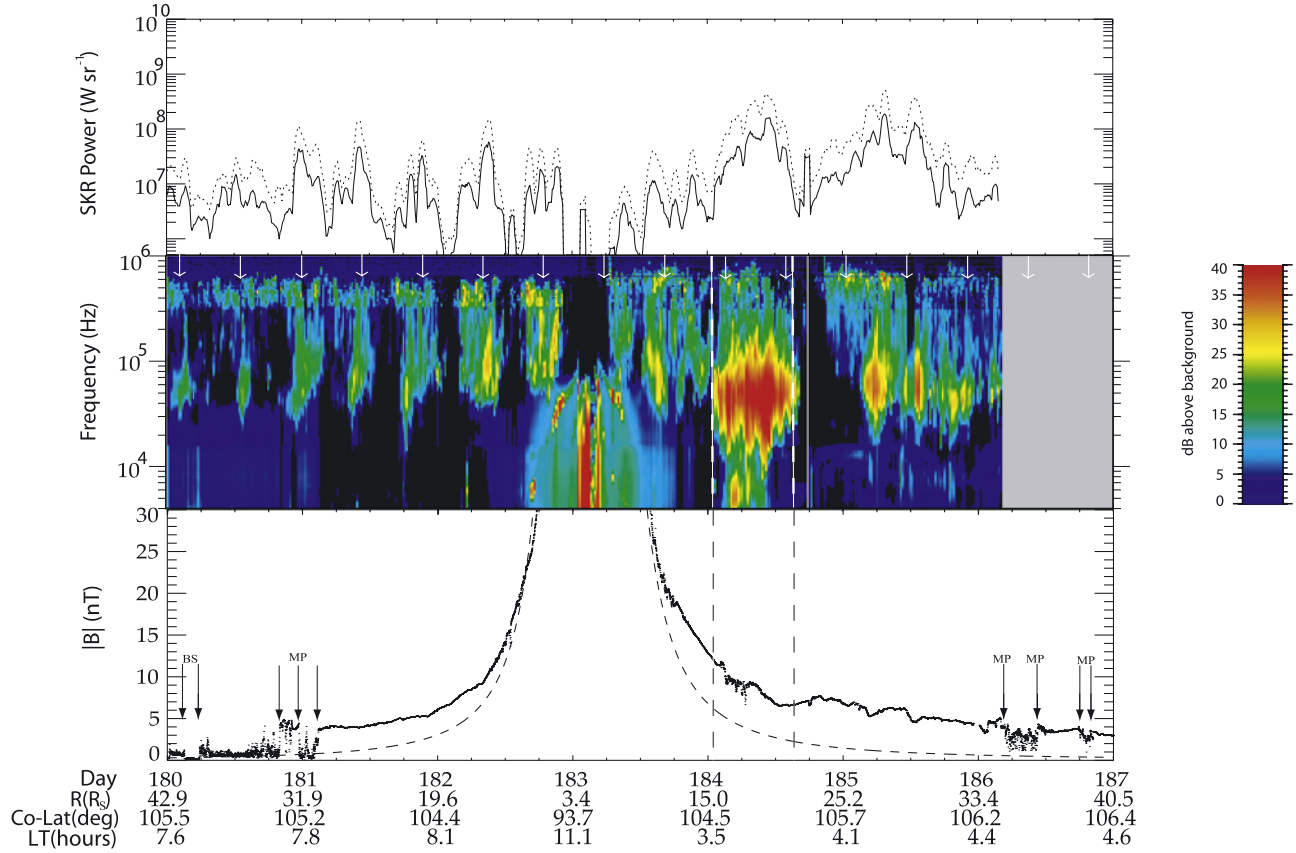

Figure 5. Cassini SKR and magnetic field data for days 180–186, encompassing the SOI fly-through of Saturn's magnetosphere. (top and middle) Similar to Figure 1, though with a data gap for much of the final day. (bottom) Magnitude of the magnetic field strength over the same interval, with the dashed curve showing the strength of the internal field of the planet from the SPV model. Vertical dashed lines indicate the interval of the first major burst of SKR observed on the outbound pass. In Figure 5 (bottom) the vertical arrows marked "BS" and "MP" indicate bow shock and magnetopause crossings, respectively. Information on spacecraft position is given at the bottom, specifically the distance from the planet (R_S), the colatitude relative to the magnetic and spin axis (degrees), and the local time (hours).

of the auroral and SKR events relate to the time of arrival of the CIR compression, but we suppose that they must generally be coincident to within a few hours. Noting from the results of *Jackman et al.* [2004, 2005] and from Figures 1 and 2 that compression regions typically last for several days following the arrival of the initial forward shock, we may then expect compressive effects to be present from day 184 throughout the remainder of the outbound pass and into the SKR data gap, but to relax toward the end of solar rotation 3 in Figure 3, consistent with the outbound boundary locations observed in the magnetometer data [*Dougherty et al.*, 2005].

4.2. SKR Observations During the SOI Fly-Through

[23] With the HST-Cassini campaign data as background, we now consider the magnetic field and SKR observations obtained during the SOI fly-through interval in more detail. In Figure 5 we show these data in the same format as Figure 1, over the interval from day 180 to 186. These data thus span the interval from the bow shock crossings and magnetopause crossings observed inbound on days 180 and 181 (shown by the vertical arrows marked "BS" and "MP," respectively), to the first magnetopause crossings observed outbound on day 186 (marked similarly). Closest approach to the planet occurred at 0239 UT on day 183. The major distinction between Figures 1 and 5 therefore is that the magnetic field data in Figure 1 (bottom) shows the IMF upstream of Saturn, while that in Figure 5 generally corresponds to Saturn's magnetospheric field. We note that as in Figures 1 and 2, the SKR power values in Figure 5 (top) have generally been derived using an assumed source at the center of the planet, except for the near-planet interval on days 182.5–183 when the goniometer method was employed as mentioned above. We also note that the gray segment of the frequency-time spectrogram on the right side of Figure 5 (middle) corresponds to the start of the extended science data gap mentioned above.

[24] If we first examine the SKR data in Figures 5 (top) and 5 (middle), it can be seen that planetary-modulated SKR emissions spanning the frequency range from ~40 to ~600 kHz are present throughout the inbound pass. As in Figure 1, a series of vertical arrows has been drawn in Figure 5 (middle), separated from each other by fixed intervals of 10.75 hours and adjusted to coincide with peaks in the emission on the inbound pass (account being taken also of data from earlier intervals than that shown). An

~8 hours gap in observed SKR emissions then spanned the interval of closest approach, while waves in the in situ plasma medium intruded into the band at frequencies below the upper hybrid resonance, reaching ~100 kHz near closest approach [*Gurnett et al.*, 2005]. A short (~1.5 hours) interval of very intense noise was also observed near closest approach, extending from low frequencies to several tens of kHz, which was associated with the firing of the rocket motor which placed Cassini into orbit around Saturn. Power in these non-SKR emissions is efficiently excluded from the values shown in Figure 5 (top) through examination of their polarization characteristics. Observations of SKR emissions were resumed ~4 hours after closest approach, these being of similar normalized amplitude and frequency range as those observed on the inbound pass. They also appear initially to be modulated in phase with the inbound pass, though the considerable structure observed in the emissions renders this conclusion somewhat uncertain. Voyager observations have previously established, however, that the phase of SKR modulations does not depend on the spacecraft longitude, between the inbound and outbound passes [e.g., *Kaiser et al.*, 1984]. A major burst of SKR emission then started at the beginning of day 184, extending to frequencies below 4 kHz, peaking in intensity at $\sim 5 \times 10^8$ W sr^{-1} (over the full 4–1000 kHz frequency band), and lasting for ~14 hours. We note from the arrows in Figure 5 (middle) that this burst occurred essentially in antiphase with the previous planetary modulation, such that relative minima in power occurred near expected maxima at the start and end of the burst, while peak powers were observed near an expected minimum. Following this burst an ~11 hours interval of low SKR-band power was then observed at Cassini, before further structured high-power bursts were observed on day 185, which were again not generally in phase with the inbound planetary modulation.

[25] Comparison of these SKR observations with those for 24–30 January 2004 in Figure 1 shows a number of similarities. In both cases a prior interval of relatively low-power planetary-modulated SKR emission was disrupted by several-hour bursts of high power emission which extend to lower frequencies than before and which do not observe the prior planetary phasing. Also in both cases, the initial high-power burst was followed by a several hour interval of low SKR power prior to the occurrence of further high-power bursts. As indicated by the January 2004 Ulysses observations mentioned in section 2, however, the observation of low powers by Cassini does not necessarily imply a global lull in emission, but perhaps only a significant change in the beaming pattern of the radiation. In the January 2004 interval the subsequent bursts eventually resumed the prior planetary phasing ~2 days after onset, a feature that cannot be followed in the SOI interval due to the extended data gap that followed. Planetary-modulated emissions were again present, however, when science data collection was resumed on day 195. In the January interval we know that these disturbed SKR emission features were associated with a CIR compression of the magnetosphere, and related major auroral disturbances illustrated in Figures 1 and 2. In view of the similarities noted above, it thus seems reasonable to suppose that the SKR burst events observed on the outbound pass in Figure 5 were related similarly to the anticipated CIR compression during the SOI fly-through. We thus infer that the inbound pass took place before the arrival of the compression region and in the absence of major auroral disturbance, while the outbound pass, certainly after the beginning of day 184, took place during conditions of compression, and in the presence of auroral and SKR disturbance of a similar nature to that observed during the HST-Cassini campaign shown in Figures 1 and 2.

5. Magnetic Field Observations During the SOI Fly-Through

[26] As shown in section 2 and previously by *Clarke et al.* [2005] and *Kurth et al.* [2005], the CIR-related SKR disturbances observed during the January 2004 HST-Cassini campaign were accompanied by bright auroral displays that are indicative of the injection of hot plasma into the nightside-dawn outer magnetosphere, followed by subcorotation around the planet via dawn to noon and beyond [*Cowley et al.*, 2005]. Given this scenario, it is of interest to examine whether related features were observed in situ by Cassini as it traversed the predawn magnetosphere during the interval of SKR disturbance on its outbound pass. We thus examine the magnetospheric magnetic field strength data shown in Figure 5 (bottom) to determine whether such features were observed. The dashed line in Figure 5 (bottom) also shows the magnitude of the internal field alone determined from the Saturn-Pioneer-Voyager (SPV) model of *Davis and Smith* [1990], for purposes of comparison. Information on the position of the spacecraft during the fly-through is indicated at the bottom of Figure 5, showing the distance from the planet (R_S), the colatitude relative to the magnetic and spin axis (degrees), and the local time (hours). It can be seen that the spacecraft approached the planet from a radial range of ~43 R_S at the start of the interval, at a local time of ~7.6 hours in the postdawn sector, and receded to a radial range of ~41 R_S at the end of the interval, at a local time of ~4.5 hours in the predawn sector. With the exception of a short interval near closest approach, the spacecraft was also consistently located south of the planet's equatorial plane, at a latitude of $\sim -15°$.

[27] If we first examine the magnetic field data from the inbound pass, no evidence can be seen that would suggest the occurrence of a sudden magnetospheric compression during the interval, at least up to the second half of day 182. Such a compression would be expected to result in an increase in field strength of a few nT over an interval of several tens of minutes, and clearly none is evident. After the first half of day 182, however, the rapid rise in field strength to large values near closest approach would render such an effect very hard to discern. Overall, however, these data are consistent with the conclusions of section 4 above, that the inbound pass took place prior to the arrival of the CIR compression.

[28] Turning therefore to the data from the outbound pass, we note that near the middle of day 183, when the field magnitude returned to within the range of the plot, the spacecraft was located at a radial distance of ~9 R_S within a region of warm corotating plasma in which the density decreased slowly with increasing distance [*Young et al.*, 2005]. The presence of this warm middle magnetosphere

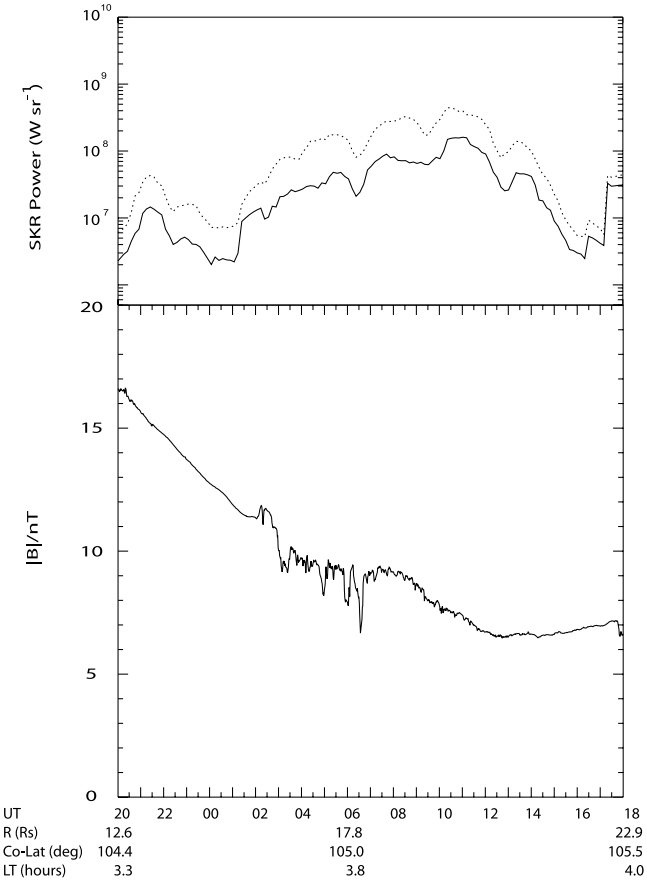

Figure 6. Cassini SKR and magnetic field strength data as in Figure 5 but plotted on an expanded time base for the interval 2000 UT on day 183 to 1800 UT on day 184. Spacecraft position data are given at the bottom.

plasma is indicated in the magnetic field data by the small-scale variations that occurred in the field strength, as is also evident in the corresponding region of the inbound pass [*Dougherty et al.*, 2005]. At 2130 UT on day 183 the spacecraft then passed into a low-density region of quiet field at a radial distance of ~13.6 R_S, which we take from an examination of the spacecraft location and the field direction to correspond to the tail lobe. Mapping of model field lines from the spacecraft into the polar ionosphere yields a colatitude of ~15° at this time, which is plausibly close to the boundary of open and closed field lines, as inferred from prior auroral data. At ~0300 UT on day 184, however, at a radial distance of ~16.5 R_S, the magnetic field data indicate that the spacecraft was again engulfed by hot plasma. This is indicated by a sudden reduction in the field strength, and subsequent rapid variations in the field indicative of the presence of a high-beta plasma. Comparison with the SKR data in Figures 5 (top) and 5 (middle) shows that these effects occurred in direct temporal correspondence with the large burst of SKR emission that began at the start of day 184, bracketed by the vertical dashed lines in Figure 5.

[29] The magnetic field data spanning the SKR burst are shown on an expanded time base in Figure 6 (bottom), together with the SKR power data in Figure 6 (top). It can be seen that a small sudden increase in the field strength occurred shortly after 0200 UT on day 184, which might represent the effect of a sudden magnetospheric compression. Following this, the field underwent a large sudden reduction in strength centered on ~0300 UT, from a peak of ~11.5 nT to a trough of ~9.5 nT, this representing a reduction in the magnetic pressure by ~30%. Following this the field underwent large irregular variations in strength over the following ~4 hours, after which the field fluctuations continued but at diminishing amplitudes. These data thus clearly indicate the sudden appearance of hot plasma at the spacecraft at and after ~0300 UT, in association with the SKR burst shown in Figure 6 (top). We suggest the most likely scenario is that the hot plasma was formed by tail dynamics (e.g., possibly reconnection) at larger distances down the tail, and was then injected along the previously open field lines toward the planet, where it was observed by the spacecraft in the relatively near-planet predawn magnetosphere. This scenario is consistent with the picture suggested by *Cowley et al.* [2005], who proposed that the CIR-related auroral disturbances observed during the HST-Cassini campaign in January 2004, discussed in section 2, were due to compression-induced reconnection in the magnetospheric tail which closed a significant fraction of the previously open magnetic flux. Detailed examination of the Cassini plasma data for this interval thus becomes a priority, but is beyond the scope of the study presented here. We finally note in Figure 5 that further variations of the tail field were also observed on day 185, after the initial SKR-related event discussed here, and that these too appear to be temporarily related to the subsequent high-power SKR bursts that were observed on this day.

6. Summary

[30] In this paper we have employed concurrent magnetic field and SKR emission data from the Cassini spacecraft to discuss the nature of the interplanetary conditions during the SOI fly-through of Saturn's magnetosphere, and their probable connection with dynamic phenomena observed inside the magnetosphere during the pass. Examination of the IMF data over two solar rotations before and two solar rotations after the fly-through shows that a CIR compression region and embedded HCS crossing is expected to have impinged on Saturn's magnetosphere at some time during the 5-day pass (between days 181 and 186), though these contextual data do not provide a more detailed indication of the expected event timing. Investigation of the direction of the field observed in the inbound and outbound magnetosheath and solar wind does confirm however, that a crossing of the HCS of appropriate sign (from a toward to an away sector) did indeed occur during the interval the spacecraft was located inside the magnetosphere, thus providing strong corroborative evidence that a CIR compression impinged on the magnetosphere at some time during the fly-through. This inference is also supported by the observed locations of the bow shock and magnetopause, which were relatively expanded on the inbound pass and compressed (at least initially) on the outbound pass, relative to expectations at the local times concerned [*Dougherty et al.*, 2005].

[31] Given these inferences, we have then overviewed the results obtained during the HST-Cassini campaign in January 2004, when detailed observations were made of the

SKR and auroral emissions associated with the arrival at Saturn of a CIR compression region. These observations show that high-power bursts of radio emission followed the arrival of a CIR compression, as discussed previously by *Kurth et al.* [2005]. These bursts disrupted the preexisting pattern of planetary-modulated emission, which was then gradually reestablished after an interval of 2–3 days. During this event, two ~8 hours bursts of high SKR power were observed, each characteristically extending to lower frequencies than before and separated by a ~23 hours interval (i.e., two planetary rotations) of relative SKR quiet as seen at Cassini. In view of the continued observation of SKR by Ulysses during this interval, however, this relative quiet could be due to an alteration in the beaming pattern, rather than to an overall absence of SKR. The concurrent HST observations show that the burst intervals were associated with intense UV auroral activity at Saturn, involving the poleward expansion of bright emissions into the dawn sector, followed by rotation to noon and later local times, forming a spiral pattern. *Cowley et al.* [2005] have suggested that this morphology is produced by a CIR compression-induced interval of rapid open flux closure in the tail leading to hot plasma injection in the nightside magnetosphere, followed by flow around the planet in the dawn sector produced by magnetosphere-ionosphere coupling in the presence of rapid planetary rotation. Examination of concurrent SKR and IMF data from several solar rotations surrounding the SOI fly-through shows that such SKR enhancements usually occur in association with CIR compressions, in conformity with prior Voyager results, such that we associate them generally with the type of auroral activity observed during the January 2004 HST-Cassini campaign.

[32] We have then examined data from the SOI fly-through interval in some detail. We find that a HCS crossing from an away to a toward sector occurred ~9 days prior to entry into Saturn's magnetosphere, such that rarefaction region conditions following this interval prevailed at the time of entry. The SKR emissions, which were modulated at the planetary period, were correspondingly very weak during this period, and continued to be relatively weak during the inbound and early outbound passage through the magnetosphere, up until the beginning of day 184. We thus infer that the inbound pass, at least, occurred under conditions of SKR and auroral quiet, prior to the arrival of the compression. There is certainly no evidence in the in situ magnetospheric magnetic field data for the occurrence of a sudden increase in field strength that might accompany a compression of the outer magnetosphere during this interval. However, the expected in situ magnetic signature is made difficult to discern due to the large and rapidly changing field at the spacecraft during the close approach interval.

[33] Bursts of high-power SKR emission were then observed during the outbound pass, the most notable of which was a burst lasting ~14 hours which began near the start of day 184. Such bursts are of a similar character to those observed during the 24–30 January HST-Cassini campaign event, which we thus infer were related similarly to the arrival of the anticipated CIR compression region. Specifically, the main SKR bursts had comparable power to those observed during the January interval, extended to significantly lower frequencies than before and disrupted the preexisting pattern of planetary modulation, with a significant interval of quiet (as seen by Cassini) following the initial burst. Comparison with the in situ field data in the predawn magnetosphere also clearly indicates that these emissions were related to concurrent variations in the nightside magnetic field. Specifically, the major SKR burst on day 184 occurred together with the appearance of hot plasma at the spacecraft, clearly indicated in the magnetic field data as an interval of depressed and highly variable magnetic field strength, following the prior interval during which the spacecraft was located in the quiet field of the southern tail lobe. Such behavior is suggestive of the onset of tail dynamics at larger distances, possibly magnetic reconnection, which resulted in the injection of hot plasma along previously open field lines into the dawn sector magnetosphere. We suggest that this represents an in situ signature directly related to the CIR-associated auroral dynamics observed by the HST during the January 2004 campaign. The observations are consistent with the interpretive scenario suggested by *Cowley et al.* [2005], in which the CIR compression induces an interval of rapid reconnection in the tail, which injects hot plasma into the nightside magnetosphere, and from thence around the planet via dawn. We also suggest that the outbound SKR bursts were associated with the same CIR-related tail dynamics, whose timing overrode that of the unknown process that usually modulates the SKR emission near the planetary period. The extension of the SKR emission to lower frequencies in such events could then result from the enhanced field-aligned currents flowing between the magnetosphere and ionosphere, which cause the discrete auroral acceleration regions to move to higher altitudes, and hence to smaller gyrofrequencies, in order to enhance the precipitating magnetospheric electron flux. We believe that these data thus provide the first evidence of a specific link between SKR emission features and in situ dynamics inside Saturn's magnetosphere.

[34] **Acknowledgments.** Work at Leicester was supported by PPARC grant PPA/G/O/2003/00013. EJB was supported by PPARC postdoctoral fellowship PPA/P/S/2002/00168. This work employs observations made by the NASA/ESA Hubble Space Telescope, obtained at the Space Telescope Science Institute, which is operated by the AURA Inc for NASA.

[35] Shadia Rifai Habbal thanks Michael D Desch and Patrick H M Galopeau for their assistance in evaluating this paper.

References

Boudouridis, A., E. Zesta, L. R. Lyons, P. C. Anderson, and D. Lummerzheim (2003), Effect of solar wind pressure pulses on the size and strength of the auroral oval, *J. Geophys. Res.*, *108*(A4), 8012, doi:10.1029/2002JA009373.

Boudouridis, A., E. Zesta, L. R. Lyons, P. C. Anderson, and D. Lummerzheim (2004), Magnetospheric reconnection driven by solar wind pressure fronts, *Ann. Geophys.*, *22*, 1367.

Bunce, E. J., S. W. H. Cowley, C. M. Jackman, J. T. Clarke, F. J. Crary, and M. K. Dougherty (2005), Cassini observations of the interplanetary medium upstream of Saturn and their relation to Hubble Space Telescope auroral data, *Adv. Space Res.*, in press.

Chua, D., G. Parks, M. Brittnacher, W. Peria, G. Germany, J. Spann, and C. Carlson (2001), Energy characteristics of auroral electron precipitation: A comparison of substorms and pressure pulse related auroral activity, *J. Geophys. Res.*, *106*, 5945.

Clarke, J. T., et al. (2005), Morphological differences between Saturn's ultraviolet aurorae and those of Earth and Jupiter, *Nature*, *433*, 717.

Cowley, S. W. H., E. J. Bunce, and R. Prangé (2004), Saturn's polar ionospheric flows and their relation to the main auroral oval, *Ann. Geophys.*, *22*, 1379.

Cowley, S. W. H., S. V. Badman, E. J. Bunce, J. T. Clarke, J.-C. Gérard, D. Grodent, C. M. Jackman, S. E. Milan, and T. K. Yeoman (2005), Reconnection in a rotation-dominated magnetosphere and its relation to Saturn's auroral dynamics, *J. Geophys. Res.*, *110*, A02201, doi:10.1029/2004JA010796.

Crary, F. J., et al. (2005), Solar wind dynamic pressure and electric field as the main factors controlling Saturn's auroras, *Nature*, *433*, 720.

Crooker, N. U., et al. (1999), CIR morphology, turbulence, discontinuities, and energetic particles, *Space Sci. Rev.*, *89*, 179.

Davis, L., Jr., and E. J. Smith (1990), A model of Saturn's magnetic field based on all available data, *J. Geophys. Res.*, *95*, 15,257.

Desch, M. D. (1982), Evidence for solar wind control of Saturn radio emission, *J. Geophys. Res.*, *87*, 4549.

Desch, M. D., and H. O. Rucker (1983), The relationship between Saturn kilometric radiation and the solar wind, *J. Geophys. Res.*, *88*, 8999.

Dougherty, M. K., et al. (2004), The Cassini magnetic field investigation, *Space Sci. Rev.*, *114*, 331.

Dougherty, M. K., et al. (2005), Cassini magnetometer observations during Saturn orbit insertion, *Science*, *307*, 1266.

Galopeau, P. H. M., and A. Lecacheux (2000), Variations of Saturn's radio rotation period measured at kilometer wavelengths, *J. Geophys. Res.*, *105*, 13,089.

Galopeau, P., P. Zarka, and D. LeQuéau (1989), Theoretical model of Saturn's kilometric radiation spectrum, *J. Geophys. Res.*, *94*, 8739.

Galopeau, P. H. M., P. Zarka, and D. LeQuéau (1995), Source location of Saturn's kilometric radiation: The Kelvin-Helmholtz instability hypothesis, *J. Geophys. Res.*, *100*, 26,397.

Gérard, J.-C., V. Dols, D. Grodent, J. H. Waite, G. R. Gladstone, and R. Prangé (1995), Simultaneous observations of the Saturnian aurora and polar haze with the HST/FOC, *Geophys. Res. Lett.*, *22*, 2685.

Gérard, J.-C., D. Grodent, J. Gustin, A. Saglam, J. T. Clarke, and J. T. Trauger (2004), Characteristics of Saturn's FUV aurora observed with the Space Telescope Imaging Spectrograph, *J. Geophys. Res.*, *109*, A09207, doi:10.1029/2004JA010513.

Gosling, J. T. (1996), Corotating and transient solar wind flows in three dimensions, *Ann. Rev. Astron. Astrophys.*, *34*, 35.

Gosling, J. T., and V. J. Pizzo (1999), Formation and evolution of corotating interaction regions and their three dimensional structure, *Space Sci. Rev.*, *89*, 21.

Grodent, D., J.-C. Gérard, S. W. H. Cowley, E. J. Bunce, and J. T. Clarke (2005), Variable morphology of Saturn's southern ultraviolet aurora, *J. Geophys. Res.*, *110*, A07215, doi:10.1029/2004JA010983.

Gurnett, D. A., et al. (2004), The Cassini radio and plasma wave investigation, *Space Sci. Rev.*, *114*, 395.

Gurnett, D. A., et al. (2005), Radio and plasma wave observations at Saturn from Cassini's approach and first orbit, *Science*, *307*, 1255.

Jackman, C. M., N. Achilleos, E. J. Bunce, S. W. H. Cowley, M. K. Dougherty, G. H. Jones, S. E. Milan, and E. J. Smith (2004), Interplanetary magnetic field at ~9 AU during the declining phase of the solar cycle and its implications for Saturn's magnetospheric dynamics, *J. Geophys. Res.*, *109*, A11203, doi:10.1029/2004JA010614.

Jackman, C. M., N. Achilleos, E. J. Bunce, S. W. H. Cowley, and S. E. Milan (2005), Structure of the interplanetary magnetic field during the interval spanning the first Cassini fly-through of Saturn's magnetosphere and its implications for Saturn's magnetospheric dynamics, *Adv. Space Res.*, in press.

Kaiser, M. L., M. D. Desch, J. W. Warwick, and J. B. Pearse (1980), Voyager detection of non-thermal radio emission from Saturn, *Science*, *209*, 1238.

Kaiser, M. L., M. D. Desch, W. S. Kurth, A. Lecacheux, F. Genova, B. M. Pedersen, and D. R. Evans (1984), Saturn as a radio source, in *Saturn*, edited by T. Gehrels and M. S. Matthews, p. 378, Univ. of Ariz. Press, Tucson.

Kurth, W. S., et al. (2005), An Earth-like correspondence between Saturn's auroral features and radio emission, *Nature*, *433*, 722.

Lecacheux, A., and F. Genova (1983), Source location of Saturn kilometric radio emission, *J. Geophys. Res.*, *88*, 8993.

Meurant, M., J.-C. Gérard, C. Blockx, B. Hubert, and V. Coumans (2004), Propagation of electron and proton shock-induced aurora and the role of the interplanetary magnetic field and solar wind, *J. Geophys. Res.*, *109*, A10210, doi:10.1029/2004JA010453.

Milan, S. E., S. W. H. Cowley, M. Lester, D. M. Wright, J. A. Slavin, M. Fillingim, C. W. Carlson, and H. J. Singer (2004), Response of the magnetotail to changes in the open flux content of the magnetosphere, *J. Geophys. Res.*, *109*, A04220, doi:10.1029/2003JA010350.

Petrinec, S. M., and C. T. Russell (1996), Near-Earth magnetotail shape and size as determined from the magnetopause flaring angle, *J. Geophys. Res.*, *101*, 137.

Prangé, R., L. Pallier, K. C. Hansen, R. Howard, A. Vourladis, R. Courtin, and C. Parkinson (2004), A CME-driven interplanetary shock traced from the Sun to Saturn by planetary auroral storms, *Nature*, *432*, 78.

Sigwarth, J. B., L. A. Frank, and N. J. Fox (2000), The effect of a dynamic pressure pulse in the solar wind on the auroral oval, total open magnetic flux of the polar cap and the auroral ionosphere, paper presented at 33rd COSPAR Scientific Assembly, Comm. On Space Res., Warsaw, Poland.

Trauger, J. T., et al. (1998), Saturn's hydrogen aurora: Wide field and planetary camera: 2. Imaging from the Hubble Space Telescope, *J. Geophys. Res.*, *103*, 20,237.

Young, D. T., et al. (2005), Composition and dynamics of plasma in Saturn's magnetosphere, *Science*, *307*, 1262.

Zarka, P. (1998), Auroral radio emissions at the outer planets: Observations and theories, *J. Geophys. Res.*, *103*, 20,159.

N. Achilleos, Blackett Laboratory, Imperial College, London SW7 2BZ, UK.

E. J. Bunce, S. W. H. Cowley, and C. M. Jackman, Department of Physics and Astronomy, University of Leicester, Leicester LE1 7RH, UK. (cj47@ion.le.ac.uk)

B. Cecconi and W. S. Kurth, Department of Physics and Astronomy, University of Iowa, Iowa City, IA 52242, USA.

J. T. Clarke, Department of Astronomy, Boston University, 725 Commonwealth Avenue, Boston, MA 02215, USA.

P. Zarka, LESIA, Observatoire de Paris, F-92195 Meudon, France.